

# Effect of SiC Concentration on Microstructure and Properties of Ni-Co/SiC Nanocomposites Fabricated by Pulse Electrodeposition

Tianxiang Liu<sup>1\*</sup>, Chunyang Ma<sup>2,\*</sup>, Qiang Li<sup>2</sup>, Jun Li<sup>3</sup>, Fafeng Xia<sup>2</sup>, Chaoyu Li<sup>2</sup>

<sup>1</sup> College of Engineering, Heilongjiang Bayi Agricultural University, Daqing 163319, China;

<sup>2</sup> College of Mechanical Science and Engineering, Northeast Petroleum University, Daqing 163318, China;

<sup>3</sup> State Grid Integrated Energy Service Group Co. LTD, Beijing 100052, China

\*E-mail: [chunyangandma1@163.com](mailto:chunyangandma1@163.com)

Received: 1 August 2020 / Accepted: 12 September 2020 / Published: 31 October 2020

---

In this article, Ni-Co/SiC nanocomposites were successfully deposited by pulse current electrodeposition using modified nickel and cobalt acid solution containing SiC nanoparticles. Effects of SiC concentration on microstructure, microhardness, and properties of Ni-Co/SiC nanocomposites were analyzed by transmission electron microscopy (TEM), scanning electron microscopy (SEM), X-ray diffraction (XRD), microhardness tests, atomic force microscopy (AFM), and electrochemical tests. The results demonstrated that SiC content in Ni-Co/SiC nanocomposites increased to 9.0 wt% when SiC concentration increased from 0 to 10 g/L. Ni-Co/SiC nanocomposites prepared at 10 g/L had the finest and most uniform microstructure compared with the others. When SiC concentration increased from 5 to 10 g/L, average grain size in Ni-Co/SiC nanocomposites decreased from 67.5 nm to 58.1 nm. AFM revealed that Ni-Co/SiC nanocomposite deposited at 10 g/L possessed a fine and uniform microstructure without any evident defects such as pores or cracks. Ni-Co/SiC nanocomposite deposited at 10 g/L with average microhardness of 894.5 Hv possessed the minimum corrosion current density of  $1.6 \times 10^{-3}$  mA/cm<sup>2</sup>, demonstrating its outstanding corrosion resisting property.

---

**Keywords:** Ni-Co/SiC nanocomposite; SiC concentration; effect; corrosion resisting property

## 1. INTRODUCTION

In recent decades, Ni-Co alloys have been investigated widely because of their excellent physical and chemical properties, such as high tensile strength, surface hardness, outstanding thermal stability, and corrosion resisting property [1-5]. Li *et al.* [6] found that Ni-Co/SiC alloys could provide long-term protection for metal parts in marine environment. In addition, they also studied the effect of SiC nanoparticles on the structure and morphology of Ni-Co coatings. Pulse electrodeposition (PE) is a

simple, promising and favorable method for obtaining Ni-Co alloys containing micro- or nano-sized ceramic particles [7]. Srivastava *et al.* [8] prepared Ni-28Co-SiC nanocoatings using PE technique, and found that the wear resistance of Ni-28Co-SiC nanocoatings was better than that of Ni coatings. Baghal *et al.* [9] investigated the mechanical properties of Ni-Co/SiC composite coatings produced by PE method and revealed that SiC particles had no noticeable effect on the microhardness of Ni-Co/SiC coatings. Hefnawy *et al.* [10] analyzed the electrochemical properties of PE-deposited Ni-Co-TiN coatings and reported that the corrosion resisting property of the coatings was significantly improved by adding TiN particles.

SiC nanoparticles are inorganic ceramic powders with an average particle size of less than 100 nm [11-14]. SiC nanoparticles are usually deposited into metal-based coatings as the reinforcement phase due to their high strength, hardness, and superior wear resistance. For instance, Sun *et al.* [15] prepared Ni-SiC nanocoatings on steel substrates by using magnetic assisted PE technique. Yang *et al.* [16] studied the structure and mechanical behaviors of PE-deposited Ni-Co-SiC nanocoatings. They found that addition of SiC nanoparticles can effectively hinder the growth of Ni and Co grains. In our previous studies [17, 18], Ni-SiC nanocoatings were successfully prefabricated via PE method. Although many studies have been reported on the preparation of metal-based SiC nanocoatings, there are only a few studies in recent literature that have investigated the effect of SiC concentration on microstructure and properties of Ni-Co/SiC nanocomposites deposited by PE deposition. Furthermore, there is limited discussion on how inlaid SiC nanoparticles would determine the surface topography, microstructure, microhardness, and corrosion properties of the PE-deposited coatings. Consequently, the aim of the present work was to prepare Ni-Co/SiC nanocomposites by using PE technique and then to evaluate the effects of SiC concentration in plating bath on the surface topography, microstructure, microhardness, and wear and corrosion properties of the composites using different scientific methods, such as scanning electron microscopy (SEM), transmission electron microscopy (TEM), X-ray diffraction (XRD), atomic force microscopy (AFM), microhardness tests, and electrochemical tests.

## 2. EXPERIMENTAL

### 2.1 Electrode and electrolyte

The electrode employed for the PE electrodeposition was composed of Q235 steel (99.23% Fe, 0.15% C, 0.55% Mn, 0.04% S, and 0.03% P) with dimensions of 30×30×5 mm<sup>3</sup>. Before PE process, the electrode was polished sequentially with 200, 600, 800 and 1200 metallographic abrasive papers, and then washed in 20 g/L NaOH solution at temperature of 25 °C, and activated in 10 wt.% HCl solution for 10 s. Finally, the electrode was washed with distilled water, and dried using a DG-9036 drying box. A nickel plate with dimensions of 60×60×10 mm<sup>3</sup> was used as the anode. The distance between electrode and nickel plate was kept at 10 mm.

The bath electrolyte utilized in the PE process was a modified nickel and cobalt acid solution. The composition and plating parameters are presented in Table 1. During PE-deposition of Ni-Co/SiC nanocomposites, the average pulse current density and duty cycle were set at 7 A/dm<sup>2</sup> and 20%,

respectively. The pulse frequency and plating time were kept at 200 Hz and 50 min, respectively. In order to prevent the agglomeration of SiC nanoparticles, a LXL-400 ultrasonic stirring (ultrasonic power 200 W) was employed during the whole PE process. SiC nanoparticles were purchased from Shanghai Dachu Nanotechnology. Fig. 1 displays the TEM (Tecnai-G2-20-S-Twin) image and size distribution of SiC nanoparticles. It was found that SiC nanoparticles were concentrated together due to their surface effects [19]. Moreover, the average size of SiC nanoparticles was approximately 32.5 nm (see Fig. 1b).

**Table 1.** The electrolyte composition and plating parameters for preparing the Ni-Co/SiC nanocomposites.

Compositions and plating condition	Parameters
NiSO <sub>4</sub> ·7H <sub>2</sub> O	200 g/L
NiCl <sub>2</sub> ·6H <sub>2</sub> O	70 g/L
CoSO <sub>4</sub> ·7H <sub>2</sub> O	60 g/L
C <sub>6</sub> H <sub>5</sub> Na <sub>3</sub> O <sub>7</sub> ·2H <sub>2</sub> O	30 g/L
H <sub>3</sub> BO <sub>3</sub>	30 g/L
SiC nanoparticle	0, 5, 10, 15 g/L
pH	4.5
Temperature	50°C
Average current density	7 A/dm <sup>2</sup>
Duty cycle	20%
Frequency	200 Hz
Plating time	50 min

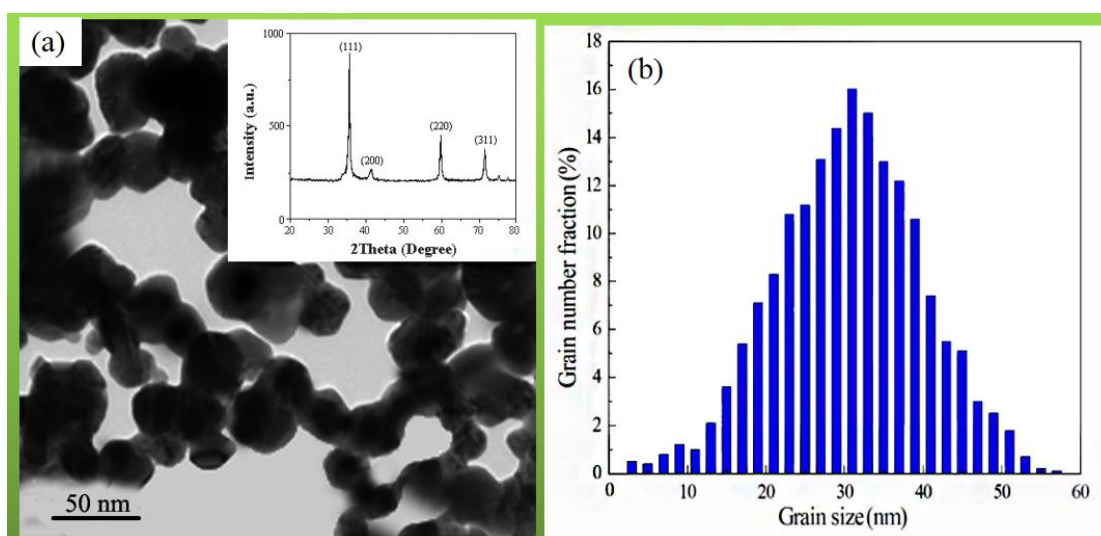


**Figure 1.** TEM image (a) and size distribution (b) of SiC powders used for depositing Ni-Co/SiC nanocomposites.

## 2.2 SEM, EDS, TEM & AFM analyses

The effects of SiC concentration in plating bath on the morphologies and microstructures of Ni-Co/SiC nanocomposites were analyzed by scanning electron microscopy (SEM, FEG450) coupled with energy dispersive spectroscopy (EDS, INCA instrument), transmission electron microscopy (TEM, Tecnai-G2-20-S-Twin), and atomic force microscopy (AFM, NT-MDT). For SEM, the scanning resolution and operating voltage and scanning resolution were 10 nm and 30 kV, respectively. For TEM, the accelerating voltage and point resolution were 150 kV and 0.19 nm, respectively. For AFM, the electron probe was a Si<sub>3</sub>N<sub>4</sub> probe with the scanning resolution of 0.2 nm. The deposition rate ( $v$ ) of Ni-Co/SiC nanocomposites was determined using Equation (1):

$$v = \frac{H}{t} \quad (1)$$

where  $H$  represents the thickness of the composite, and  $t$  represents plating time during PE deposition.

## 2.3 XRD analysis

To determine the crystalline structures of Ni-Co/SiC nanocomposites, XRD analysis was carried out via a Rigaku D/Max-2400 X-ray diffractometer with Cu-K $\alpha$  radiation. The scan rate was 0.02° per second, and the scanning range was 30° to 80°. The crystallite sizes in Ni-Co/SiC composites were calculated using the Scherrer relation [20]:

$$D = \frac{K\lambda}{\beta \cos\theta} \quad (2)$$

where  $D$  represents the size of the material,  $K$  represents the Scherrer constant,  $\lambda$  represents the radiation wavelength ( $\lambda=0.15406$  nm),  $\beta$  and  $\theta$  represent the FWHM (full width at half maximum) and angular position, respectively.

## 2.4 Microhardness measurement

The microhardness of Ni-Co/SiC nanocomposites was tested by using a 401 MVT microhardness tester. The applied loads were 50 gf and 100 gf, respectively, and the applied time was 10 s. Five measurements were carried out at different positions of each coating, and the average of these 5 readings was taken as the microhardness of the nanocomposite.

## 2.5 Corrosion resisting property test

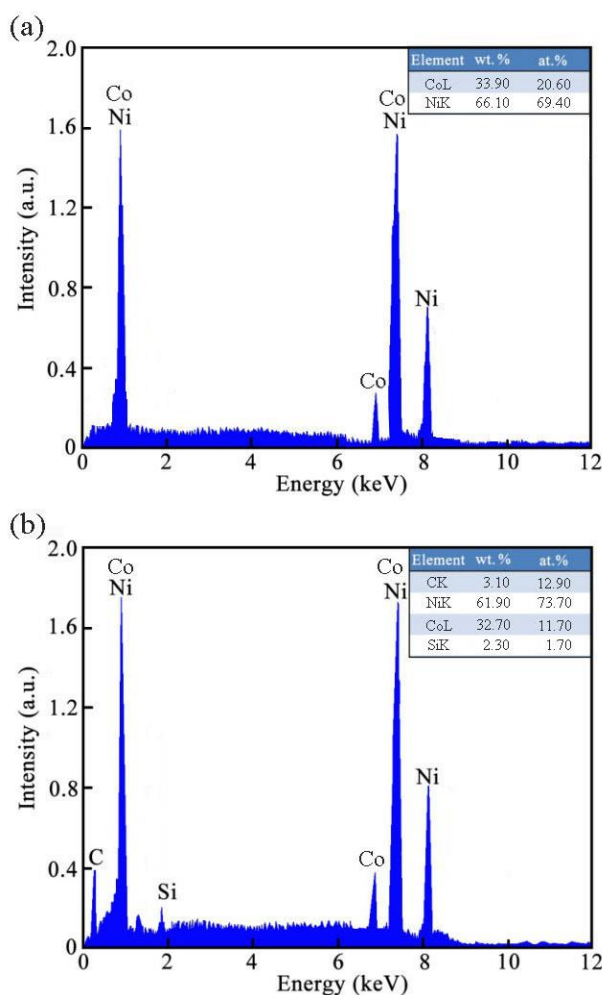
The corrosion resisting property of Ni-Co/SiC nanocomposites was characterized using a CS350 electrochemical workstation. The corrosive liquid was 3.5 wt% NaCl solution and the as-deposited specimen was used as the working electrode. The reference electrode and counter electrode were saturated calomel (SCE) and Pt electrodes. The scan rate was kept at 0.02 mV/s during the

electrochemical test. The corrosion potential and current density were obtained from Tafel curves based on one experiment. Electrochemical impedance spectroscopy (EIS) was actualized over the frequency range of  $10^{-2}$ ~ $10^5$  Hz [21, 22].

### 3. RESULTS AND DISCUSSION

#### 3.1 Effect of SiC concentration on SiC content in Ni-Co/SiC nanocomposites

Fig. 2 presents the effect of SiC concentration in plating bath on SiC content in Ni-Co/SiC nanocomposites deposited at different SiC concentrations. When no SiC nanoparticles were added to the bath electrolyte, only Ni and Co elements were detected in Ni-Co/SiC nanocomposite, which indicated that the nanocomposite was Ni-Co alloy coating. As shown in Fig. 2a, Ni-Co alloy coating contained 66.1 wt% of nickel and 33.9 wt% of cobalt. SiC content in Ni-Co/SiC nanocomposites increased to 9.0 wt.% when the SiC concentration increased from 0 to 10 g/L (see Figs. 2b-c). However, Ni-Co/SiC nanocomposites obtained at SiC concentration of 15 g/L contained only 7.7 wt% of SiC nanoparticles, demonstrating a reduction of SiC content compared with Ni-Co/SiC nanocomposite prepared at 10 g/L. These results are consistent with the result described by Sajjadnejad [23].



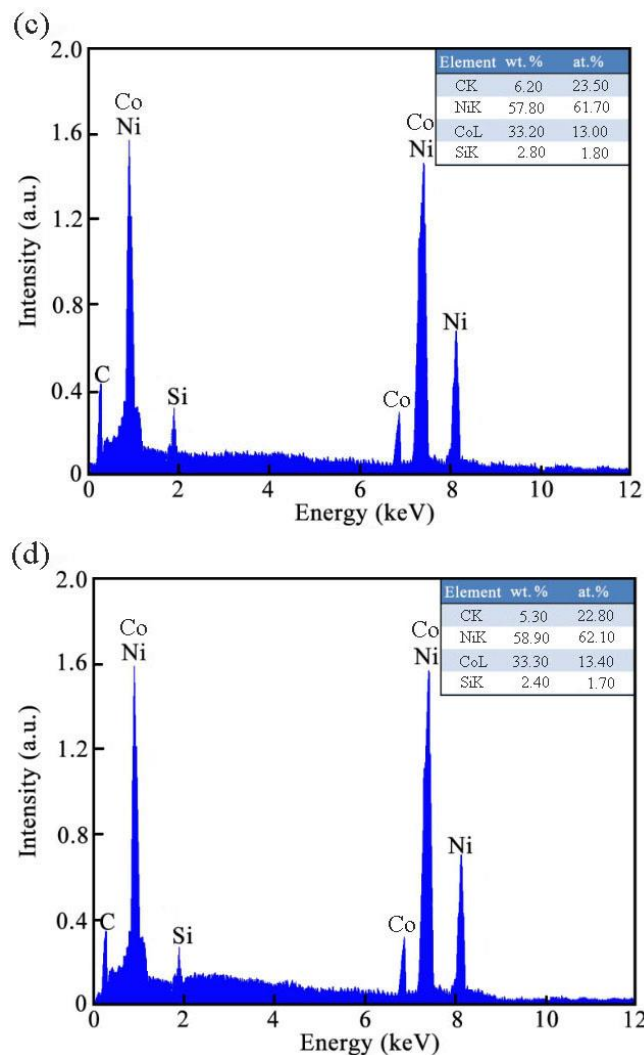


**Figure 2.** EDS spectrograms Ni-Co/SiC nanocomposites deposited at various SiC concentrations (a) 0 g/L, (b) 5 g/L, (c) 10 g/L, (d) 15 g/L, and same other parameters (average current density 7 A/dm<sup>2</sup>, duty cycle 20%, frequency 200Hz).

The following two aspects can explain these results: (1) when SiC concentration in the electroplate liquid increased from 0 to 10 g/L, SiC nanoparticles near the cathode were easily captured by nickel ions. Then, large amounts of SiC nanoparticles were co-deposited on the cathode surface with nickel ions to form Ni-Co/SiC nanocomposite. Therefore, Ni-Co/SiC nanocomposite obtained at 10 g/L had the highest SiC content. (2) when SiC concentration was too high (i.e., 15 g/L), the viscosity of the plating bath increased, leading to greater motion resistance of SiC nanoparticles. This decreased the amount of SiC nanoparticles in Ni-Co/SiC nanocomposites. As a result, SiC content in Ni-Co/SiC nanocomposite prepared at 15 g/L decreased slightly.

In order to analyze the elemental distribution of Ni-Co/SiC nanocomposite, surface scanning of Ni-Co/SiC nanocomposite deposited at 10 g/L was carried out by EDS. It was found that Ni, Co, Si, and C elements were homogeneously distributed in the nanocomposite, illustrating that SiC nanoparticles were successfully embedded into the Ni-Co matrix. This microstructure is beneficial to improve the mechanical and corrosion resisting properties of Ni-Co/SiC nanocomposite [24, 25].

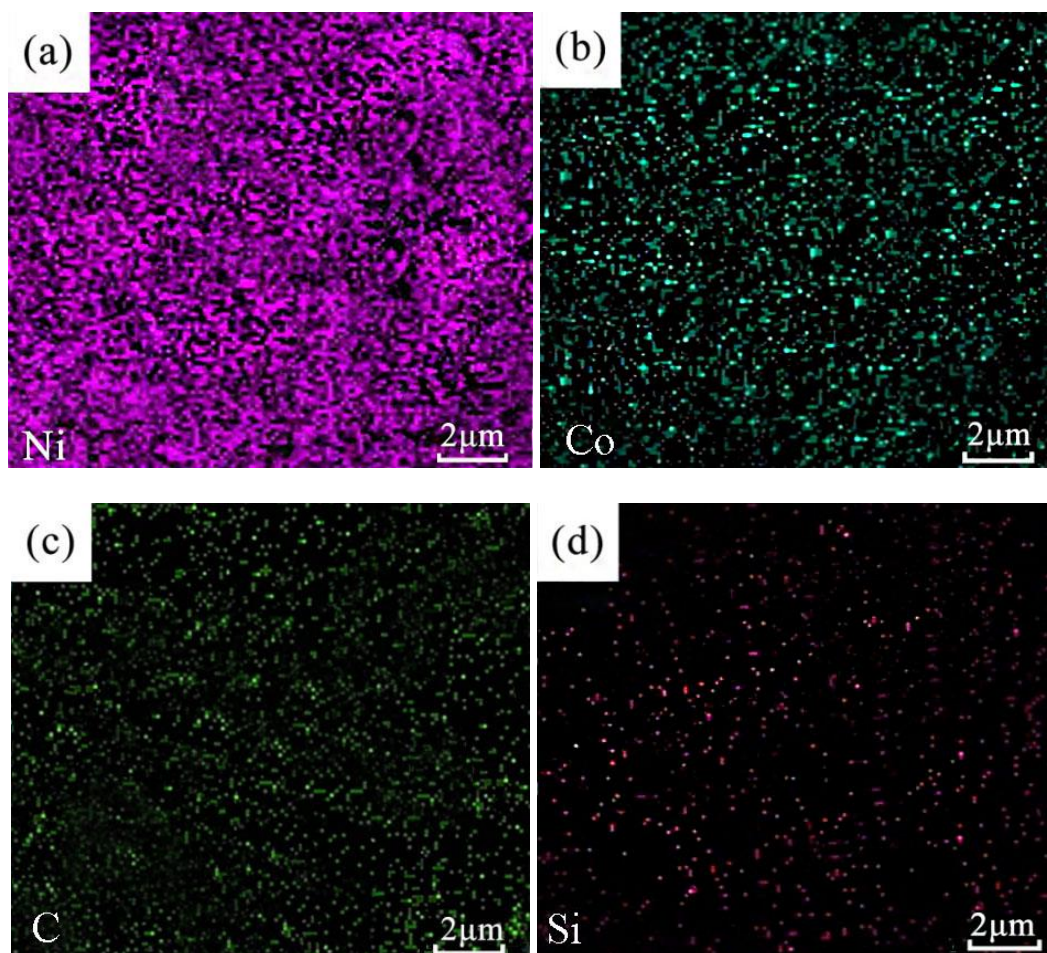


**Figure 3.** EDS spectrograms of Ni-Co/SiC nanocomposites deposited at average current density of 7 A/dm<sup>2</sup>, duty cycle of 20%, frequency of 200Hz, and SiC concentration of 10 g/L: (a) Ni, (b) Co, (c) C and (d) Si element.

### 3.2 Effect of SiC concentration on surface morphology of Ni-Co/SiC nanocomposites

As is well known, the surface morphology of metal matrix composite has an important influence on its hardness and properties, whereas the morphology of the composite is directly related to SiC concentration in plating solution [26]. Therefore, it is very important to investigate the effect of SiC concentration on surface morphology of Ni-Co/SiC nanocomposites. Fig. 4 presents the SEM surface morphologies of Ni-Co/SiC nanocomposites prepared at different SiC concentrations. A rough and grainy surface with large diamond-shaped nickel grains appeared on the coating, as shown in Fig. 4a. In contrast, Ni-Co/SiC nanocomposites deposited at 5, 10 and 15 g/L presented even, smooth, and fine-grained surfaces with uniformly distributed SiC nanoparticles. In particular, the composite prepared at 10 g/L possessed the finest and most uniform microstructure compared to the others (see Fig. 4c). As described above, when SiC concentration was 0 g/L, SiC nanoparticles had no effect on the nucleation and growth of nickel grains, and these grains grew freely during PE deposition. Therefore, Ni-Co composite showed a rough and grainy surface with larger grains. However, Ni-Co/SiC nanocomposite produced at a moderate SiC concentration (i.e. 10 g/L) possessed the maximum

SiC content (see Fig. 2c), which increased the fine grain strengthening effect of SiC nanoparticles on Ni and Co grains. Thus, the growth of Ni and Co crystals was impeded, resulting in the formation of the finest and most uniform microstructure in Ni-Co/SiC nanocomposite. This result is similar to our previous report [27].

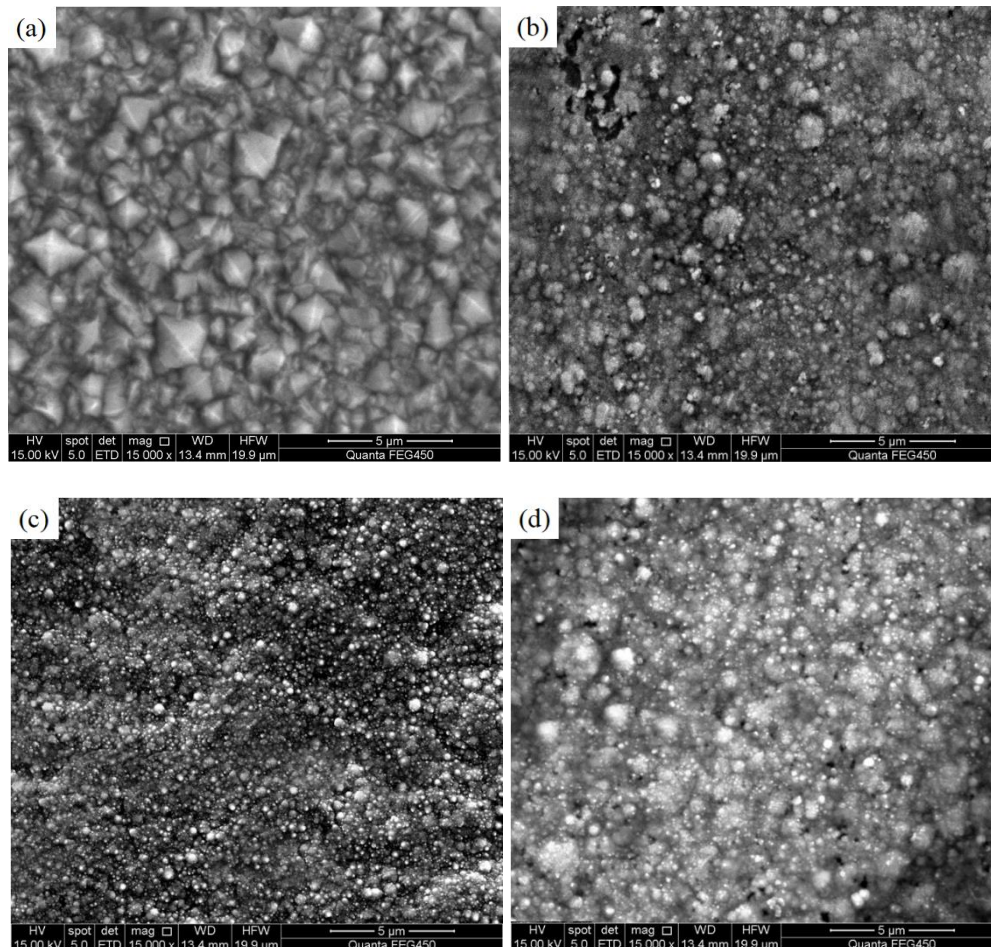


**Figure 4.** SEM surface morphologies of Ni-Co/SiC nanocomposites deposited at various SiC concentrations (a) 0 g/L, (b) 5 g/L, (c) 10 g/L, (d) 15 g/L, and same other parameters (average current density 7 A/dm<sup>2</sup>, duty cycle 20%, frequency 200Hz).

### 3.3 Effect of SiC concentration on crystalline structure of Ni-Co/SiC nanocomposites

Fig. 5 presents the XRD spectra of Ni-Co/SiC nanocomposites deposited at various SiC concentrations. When no SiC nanoparticles were added to the plating solution, the coating consisted of Ni and Co phases (see Fig. 5a). On the other hand, the nanocomposites deposited at 5, 10 and 15 g/L were composed of Ni, Co and SiC phases. With augment in SiC nanoparticle concentration from 5 to 10 g/L, XRD diffraction peaks of Ni-Co/SiC nanocomposites changed broader and smaller. This was possibly because numerous incorporated SiC nanoparticles refined the metal matrix grains [28]. However, when SiC concentration changed from 10 to 15 g/L, XRD peaks of Ni-Co/SiC films became higher and narrower compared to the coating deposited at 10 g/L. This phenomenon can be best

illustrated by the fact that the augment in SiC concentration in plating solution led to a boost in the viscosity of the plating solution, resulting in greater movement resistance for SiC nanoparticles. Therefore, SiC content in Ni-Co/SiC films decreased, which in turn decreased the inhibition effect of SiC nanoparticles on the growth of Ni and Co grains. Thus, XRD diffraction peaks of Ni-Co/SiC films changed higher and narrower with augment in SiC nanoparticle concentration from 10 to 15 g/L.

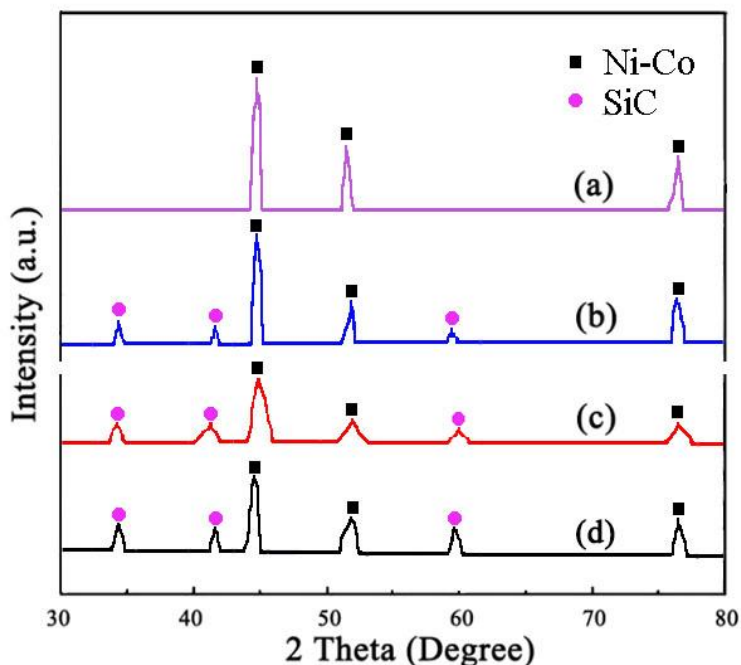


**Figure 5.** XRD patterns of Ni-Co/SiC nanocomposites deposited at various SiC concentrations (a) 0 g/L, (b) 5 g/L, (c) 10 g/L, (d) 15 g/L, and same other parameters (average current density 7 A/dm<sup>2</sup>, duty cycle 20%, frequency 200Hz).

Table 2 shows the grain sizes in Ni-Co/SiC nanocomposites calculated using Equation (2). The average grain size of Ni-Co coating without SiC nanoparticles was approximately 141.4 nm. When SiC concentration changed from 5 to 10 g/L, the average grain size in Ni-Co/SiC nanocomposites decreased from 67.5 nm to 58.1 nm. However, Ni-Co/SiC nanocomposite deposited with SiC concentration of 15 g/L possessed an average grain size of ~84.9 nm. This phenomenon can be explained as follows: (i) with augment in SiC concentration from 0 to 10 g/L, large number of SiC nanoparticles were co-deposited with Ni and Co ions into Ni-Co/SiC nanocomposites, which enhanced the fine grain strengthening effect of SiC nanoparticles on matrix crystals.

**Table 2.** Crystallite size of Ni-Co/SiC nanocomposites deposited with different SiC concentration.

SiC concentration (g/L)	Crystallite size (nm)
0	141.4
5	67.5
10	58.1
15	84.9

Thus, the grain growth in Ni-Co/SiC nanocomposites was impeded. Consequently, the average grain size in Ni-Co/SiC nanocomposites decreased from 67 nm to 58 nm as SiC concentration increased from 5 to 10 g/L. (ii) when SiC concentration increased to 15 g/L, the plating solution became viscous, resulting in increased motion resistance of SiC nanoparticles and fewer SiC nanoparticles embedded in Ni-Co/SiC nanocomposites. As a result, the effect of SiC nanoparticles on matrix grain growth decreased and the grain sizes in Ni-Co/SiC nanocomposites increased.

### 3.4 Effect of SiC concentration on microstructure of Ni-Co/SiC nanocomposites

Fig. 6 displays TEM photos of Ni-Co/SiC nanocomposites deposited at different SiC concentrations. As seen in Fig. 6a, the composite deposited without SiC nanoparticles (SiC concentration 0 g/L) contained no SiC, while Ni-Co/SiC nanocomposites deposited at 5, 10 and 15 g/L possessed numerous SiC nanoparticles.

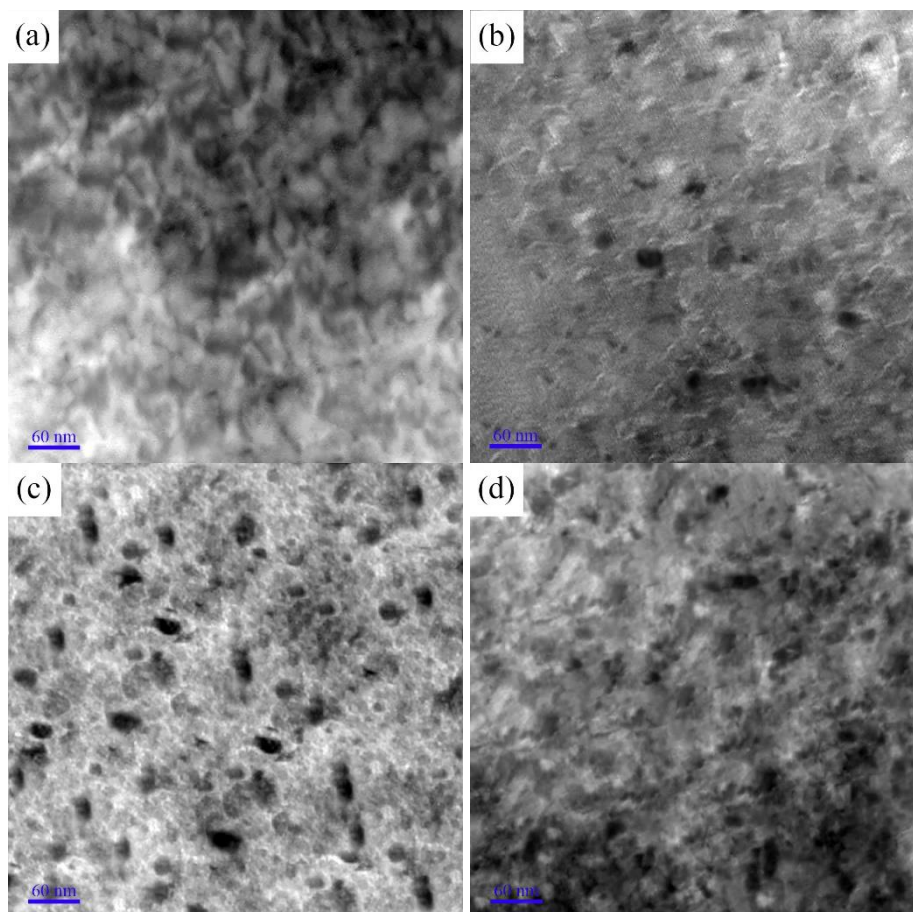


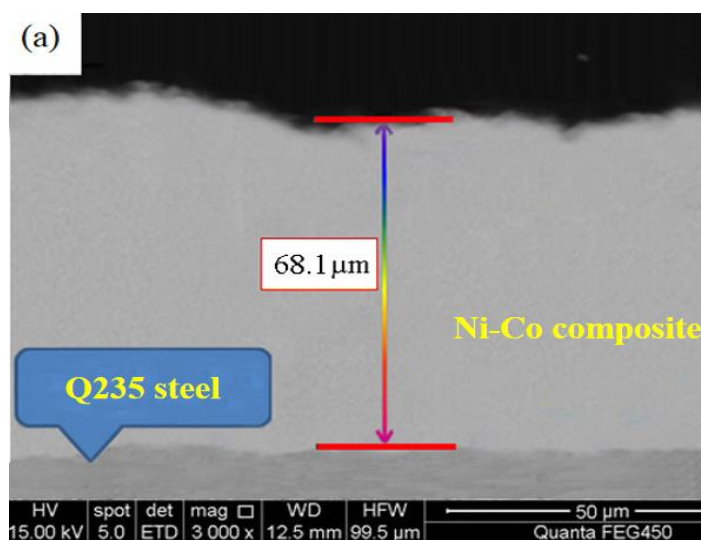
**Figure 6.** TEM images of Ni-Co/SiC nanocomposites deposited at various SiC concentrations (a) 0 g/L, (b) 5 g/L, (c) 10 g/L, (d) 15 g/L, and same other parameters (average current density 7 A/dm<sup>2</sup>, duty cycle 20%, frequency 200Hz).

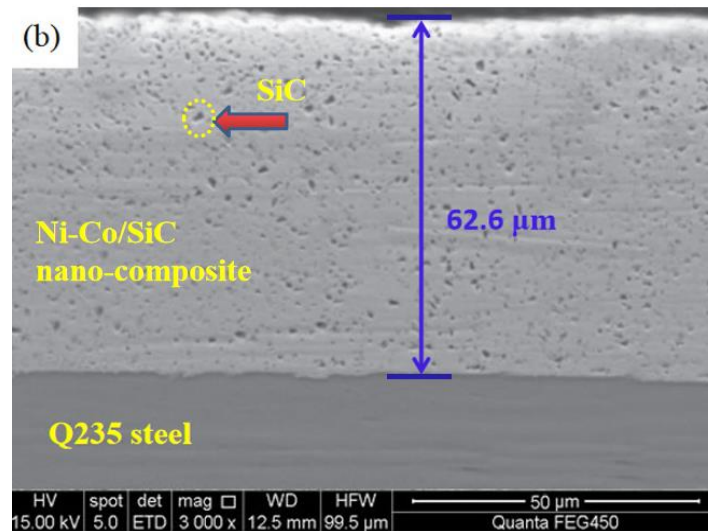
The composites prepared at 5 and 15 g/L had a rough structure, and SiC nanoparticles were agglomerated into large black clusters (see Figs. 6b and 6d). However, Ni-Co/SiC nanocomposite

produced at 10 g/L exhibited a compact and exiguous microstructure with fine matrix crystals. Moreover, the average sizes of matrix crystals and SiC nanoparticles in the nanocomposite were 58.6 nm and 33.9 nm, respectively. This result was confirmed by XRD measurement. According to the previous literature [29], coating microstructure had an important influence on the electrochemical and physical properties of the material. Therefore, appropriate microstructure can help to improve its final properties for specific applications.

### 3.5 Analysis of composite cross-sections

Fig. 7 shows the SEM cross-sections of Ni-Co/SiC nanocomposites fabricated at 0 and 10 g/L. No SiC nanoparticles were observed for the composite prepared at 0 g/L (Fig. 7a), which indicated that it was actually a Ni-Co composite. The thickness of this composite was 68.1  $\mu\text{m}$ . However, a large number of SiC nanoparticles were embedded into Ni-Co/SiC nanocomposites prepared at 10 g/L, and the thickness of this coating was 62.6  $\mu\text{m}$ . According to Equation (1), the calculated deposition rates of Ni-Co/SiC nanocomposites deposited at 0 and 10 g/L were 1.36 and 1.25  $\mu\text{m}/\text{min}$ , respectively, indicating larger deposition rate for PE-deposited Ni-Co composite compared to PE-deposited Ni-Co/SiC nanocomposites. The reason was that the low viscosity of the plating bath without SiC nanoparticles lowered the resistance of metal grain deposition. Therefore, the metal grains were deposited into the coating faster, and the deposition rate was higher.

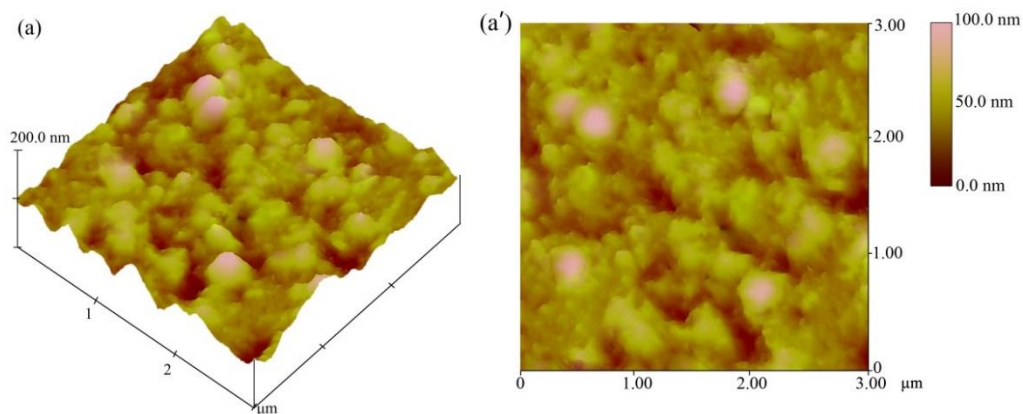




**Figure 7.** Cross-sectional images of Ni-Co/SiC nanocomposites deposited at various SiC concentrations (a) 0 g/L and (b) 10 g/L, and same other parameters (average current density 7 A/dm<sup>2</sup>, duty cycle 20%, frequency 200Hz).

### 3.6 AFM observation

Fig. 8 and Table 3 show the 2D morphology, 3D morphology and average roughness (*Ra*) of Ni-Co/SiC nanocomposite prepared at 10 g/L obtained from two random locations on the coating. Uneven microstructure was observed on the surface of the composite with an average maximum height of 85.7 nm. The *Ra* values at these sampling sites were 66.9 and 57.2 nm, respectively. In addition, AFM revealed that Ni-Co/SiC nanocomposite deposited at 10 g/L possessed a fine and uniform microstructure without any evident defects such as pores or cracks.



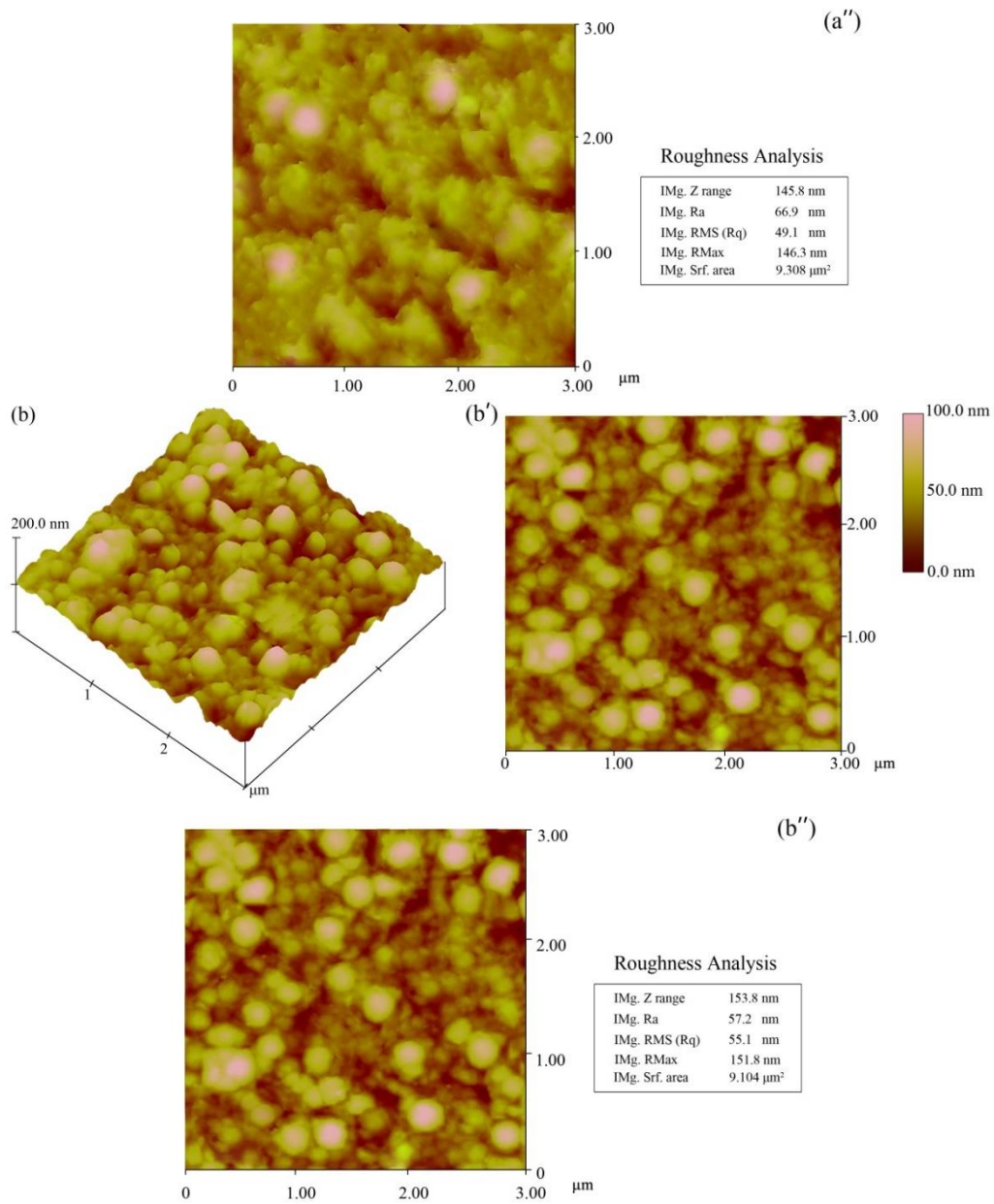


**Figure 8.** AFM images and roughness data of Ni-Co/SiC nanocomposites deposited at 10 g/L SiC concentration, average current density 7 A/dm<sup>2</sup>, duty cycle 20%, and frequency 200Hz: (a) and (b) 3D morphologies, (a') and (b') 2D morphologies, (a'') and (b'') Roughness data.

**Table 3.** The average roughness (*Ra*) of Ni-Co/SiC nanocomposites deposited at SiC concentration of 10 g/L, average current density of 7 A/dm<sup>2</sup>, duty cycle of 20%, and frequency of 200Hz.

Sample sites	Max height (nm)	<i>Ra</i> (nm)
a	85.7	66.9
b	83.4	57.2

### 3.7 Effect of SiC concentration on microhardness of Ni-Co/SiC nanocomposites

Fig. 9 and Table 4 reveal the effect of SiC concentration on microhardness of Ni-Co/SiC nanocomposites fabricated at 0, 5, 10 and 15 g/L. SiC nanoparticles in Ni-Co matrix strongly influenced the microhardness of the resulting Ni-Co/SiC nanocomposites. When SiC concentration was 0 g/L, the average microhardness of the Ni-Co composite was only 472.2 Hv. With an increase in SiC nanoparticle concentration from 5 to 10 g/L, the average microhardness of Ni-Co/SiC nanocomposites increased to 894.5 Hv. The possible reasons are: (i) SiC nanoparticles as ceramic materials have high hardness themselves [30]. The overall microhardness of Ni-Co/SiC nanocomposite was improved effectively after SiC nanoparticles were embedded in the nanocomposite. (ii) A compact and exiguous microstructure with fine matrix crystals can be produced by adding suitable SiC concentration, which increased the ability to resist external forces [31] and resulted in improved coating hardness.

However, the microhardness of Ni-Co/SiC nanocomposites decreased slightly as SiC concentration increased from 10 to 15 g/L. As previously mentioned, excess SiC concentration increased the viscosity of the plating bath, resulting in lower SiC content in Ni-Co/SiC nanocomposites. Consequently, the microhardness of the composite was reduced slightly.

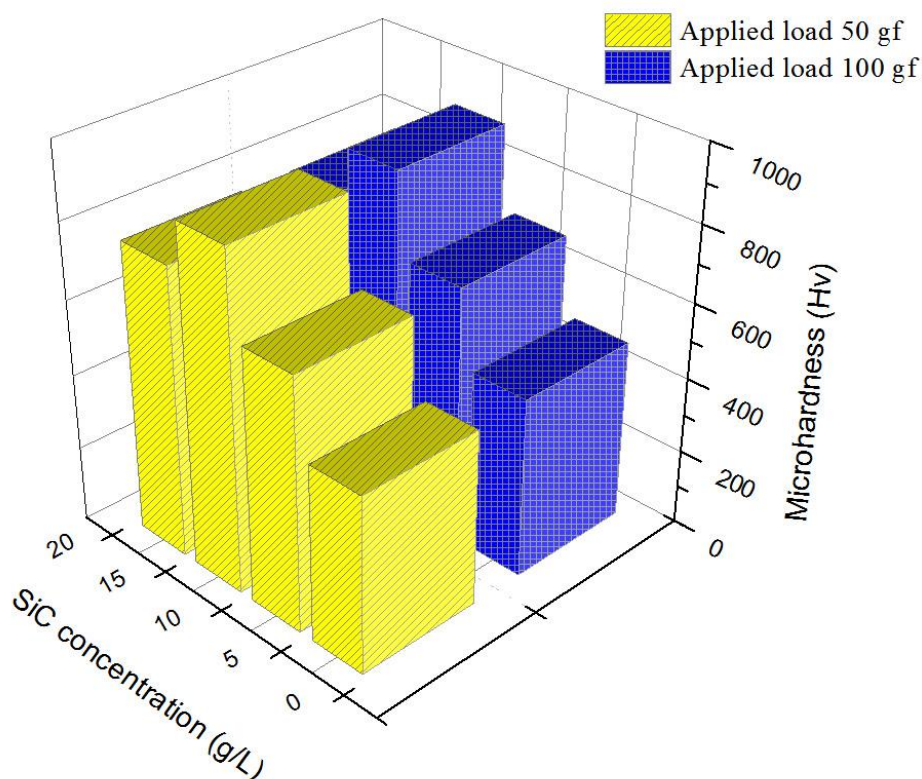


**Figure 9.** Ni-Co/SiC nanocomposites deposited at various SiC concentrations: (a) 0 g/L, (b) 5 g/L, (c) 10 g/L, and (d) 15 g/L.

**Table 4.** Microhardnesses of Ni-Co/SiC nanocomposites achieved with different applied loads.

SiC concentration (g/L)	50 gf	100 gf	Average microhardness (HV)
	Microhardness (HV)	Microhardness (HV)	
0	468.4	475.9	472.2
5	669.5	678.6	674.1
10	893.8	895.2	894.5
15	770.0	768.7	769.4

### 3.8 Effect of SiC concentration on corrosion resisting property of Ni-Co/SiC nanocomposites

The effect of SiC concentration on corrosion resisting property of Ni-Co/SiC nanocomposites was investigated by using Tafel and EIS curves. Fig. 10 shows the effect of SiC concentration on the polarization curves of the nanocomposites in 3.5 wt% NaCl solution. The corrosion current density and corrosion potential of the nanocomposites are summarized in Table 5. It can be seen that SiC concentration had a great influence on the corrosion potential of Ni-Co/SiC nanocomposite. When SiC concentration changed from 0 to 10 g/L, the corrosion potential of the composite changed from -0.479 V to -0.381 V. When SiC concentration continuously increased to 15 g/L, the corrosion potential value decreased. Therefore, it was confirmed that Ni-Co/SiC nanocomposite deposited at 10 g/L possessed the minimum corrosion current density of  $1.6 \times 10^{-3}$  mA/cm<sup>2</sup>, demonstrating supreme corrosion resisting property.

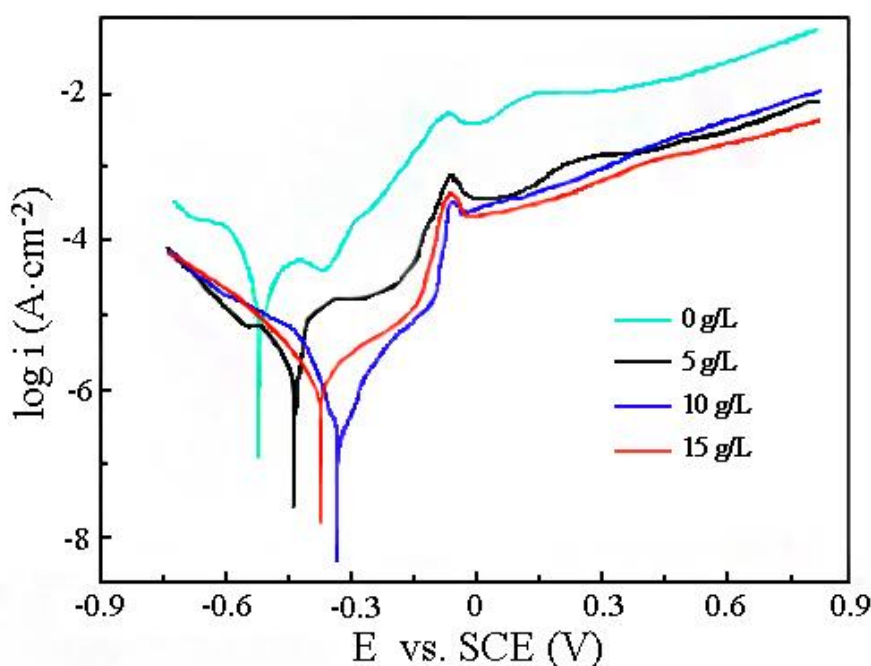


**Figure 10.** Potentiodynamic polarization curves of Ni-Co/SiC nanocomposites deposited at various SiC concentrations (a) 0 g/L, (b) 5 g/L, (c) 10 g/L, (d) 15 g/L (3.5 wt% NaCl solution, scan rate 0.02 mV/s).

**Table 5.** Electrochemical corrosion data of Ni-Co/SiC nanocomposites deposited at various SiC concentrations.

SiC concentration (g/L)	Corrosion current density (mA/cm <sup>2</sup> )	Corrosion potential (V)
0	$2.8 \times 10^{-2}$	-0.479
5	$4.1 \times 10^{-3}$	-0.442
10	$1.6 \times 10^{-3}$	-0.381
15	$2.1 \times 10^{-3}$	-0.408

Fig. 11 depicts Nyquist curves of Ni-Co/SiC nanocomposites obtained at various SiC nanoparticle concentrations, and the corrosion parameters obtained from the Nyquist curves are listed in Table 6. The terms  $R_s$ ,  $R_{ct}$  and  $C_{dl}$  represent the solution resistance, charge transfer resistance and double layer capacitance, respectively. The Nyquist plots presented moderately dented semicircles with dissimilar radii, corresponding to one-time constants [32]. As SiC concentration changed from 0 to 10 g/L, the  $C_{dl}$  value of Ni-Co/SiC nanocomposites decreased from 58.03 to 37.89  $\mu\text{F}/\text{cm}^2$ , while the  $R_{ct}$  value increased from 8125 to 51301  $\Omega \cdot \text{cm}^2$ , illustrating higher corrosion resisting property of Ni-Co/SiC nanocomposites. The minimum  $C_{dl}$  and maximum  $R_{ct}$  values of Ni-Co/SiC nanocomposites deposited at 10 g/L were 37.89  $\mu\text{F}/\text{cm}^2$  and 51301  $\Omega \cdot \text{cm}^2$ , respectively, which indicated the best corrosion resisting property among these composites. Nevertheless, the  $C_{dl}$  and  $R_{ct}$  values altered slightly as SiC concentration increased to 15 g/L.

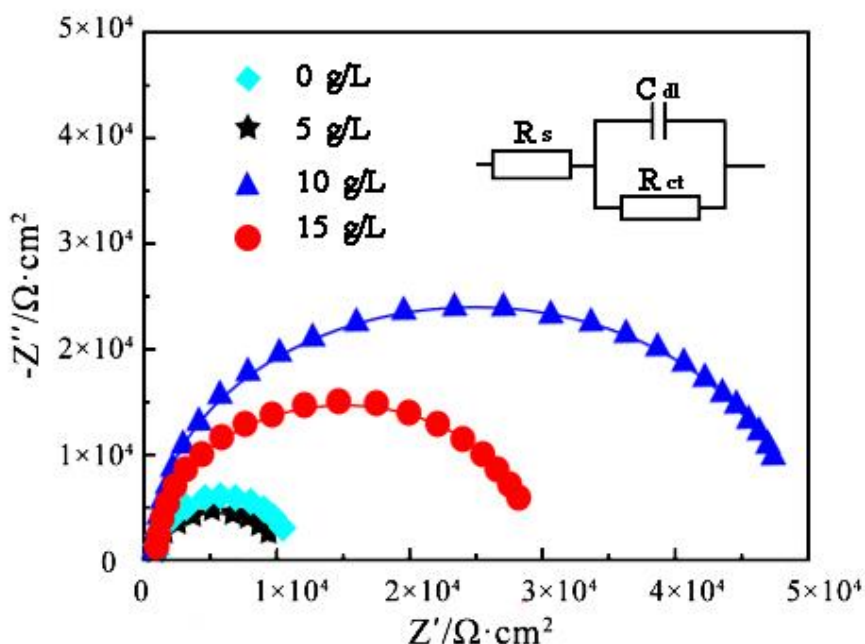
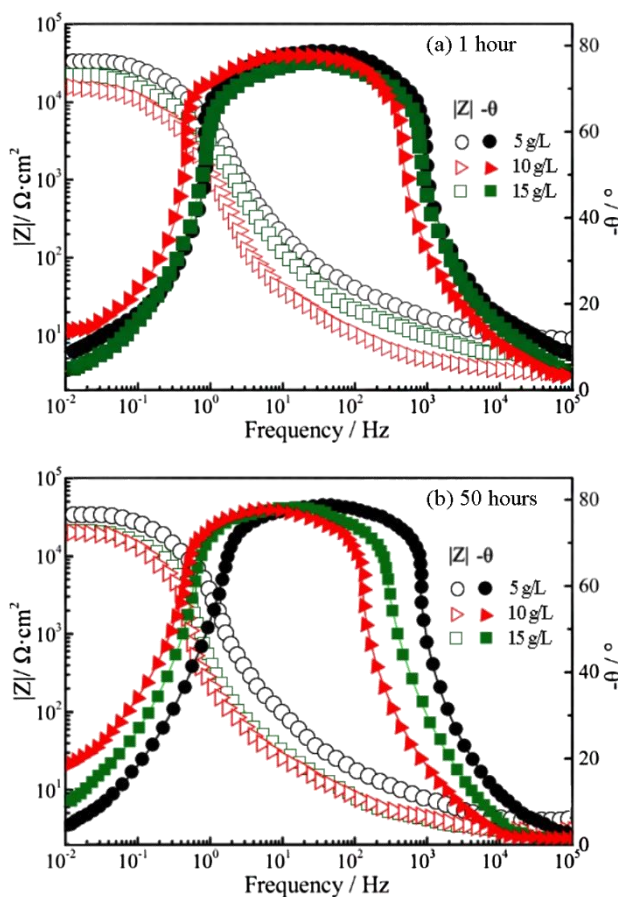


**Figure 11.** Potentiodynamic polarization curves of Ni-Co/SiC nanocomposites deposited at various SiC concentrations (a) 0 g/L, (b) 5 g/L, (c) 10 g/L, (d) 15 g/L (3.5 wt% NaCl solution, scan rate 0.02 mV/s).

**Table 6.** Corrosion parameters of Ni-Co/SiC nanocomposites deposited at various SiC concentrations.

SiC concentration (g/L)	$R_s$ ( $\Omega \cdot \text{cm}^2$ )	$R_{ct}$ ( $\Omega \cdot \text{cm}^2$ )	$Cdl$ ( $\mu\text{F}/\text{cm}^2$ )
0	6.04	8125	58.03
5	3.10	8446	67.22
10	5.27	51301	37.89
15	5.09	49012	38.38

Fig. 12 shows Bode curves of Ni-Co/SiC nanocomposites deposited at different SiC concentrations with immersion time of 1 to 100 hours. It was found that all Bode plots had a single hump-backed shape, indicating the phenomenon of similar electrochemical processes. In addition, the radius of the capacitance loop for the corresponding nanocomposites first increased and then decreased when the immersion time increased from 1 to 100 hours. Maximum modulus  $|Z|$  at approximately 5 Hz was measured for the nanocomposites obtained at SiC concentration of 10 g/L. The humps of the coatings were high and wide among all Ni-Co/SiC nanocomposites, demonstrating excellent corrosion resisting property.



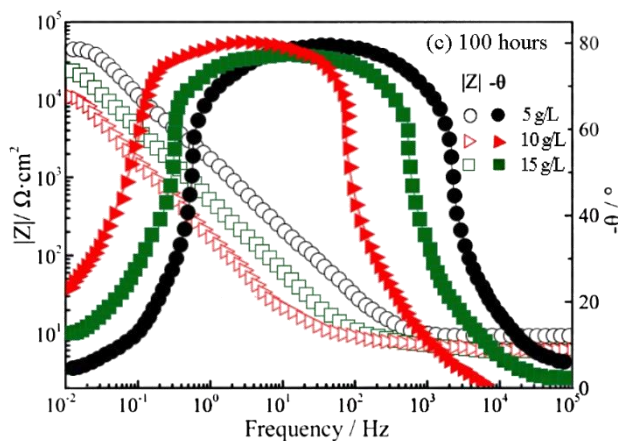


**Figure 12.** Ni-Co/SiC nanocomposites deposited at various SiC concentrations: (a) 0 g/L, (b) 5 g/L, (c) 10 g/L, and (d) 15 g/L.

#### 4. CONCLUSIONS

(1) SiC content in Ni-Co/SiC nanocomposites increased to 9.0 wt% when the SiC nanoparticle concentration increased from 0 to 10 g/L. Ni, Co, Si, and C elements were homogeneously distributed in the nanocomposite, illustrating that SiC nanoparticles were successfully embedded into the Ni-Co matrix.

(2) Ni-Co/SiC nanocomposites deposited at 5, 10 and 15 g/L presented even, smooth, and fine-grained surfaces with uniformly distributed SiC nanoparticles. In particular, the composite prepared at 10 g/L possessed the finest and most uniform microstructure compared to the others. With augment in SiC nanoparticle concentration from 5 to 10 g/L, XRD diffraction peaks of Ni-Co/SiC nanocomposites changed broader and smaller.

(3) When SiC concentration raised from 5 to 10 g/L, the average grain size in Ni-Co/SiC nanocomposites decreased from 67.5 nm to 58.1 nm. However, Ni-Co/SiC nanocomposite deposited with SiC concentration of 15 g/L possessed an average grain size of ~84.9 nm. AFM revealed that Ni-Co/SiC nanocomposite deposited at 10 g/L possessed a fine and uniform microstructure without any evident defects such as pores or cracks.

(4) When SiC concentration was 0 g/L, the average microhardness of the Ni-Co composite was only 472.2 Hv. With increase in SiC concentration from 5 to 10 g/L, the average microhardness of Ni-Co/SiC nanocomposites increased to 894.5 Hv. Ni-Co/SiC nanocomposite deposited at 10 g/L possessed the minimum corrosion current density of  $1.6 \times 10^{-3}$  mA/cm<sup>2</sup>, demonstrating supreme corrosion resisting property.

#### ACKNOWLEDGEMENTS

The research is supported by the National Natural Science Foundation of China (Grant no. 51974089).

## References

1. J. Xu, Z. Li, W. Zhu, Z. Liu, W. Liu, *Appl. Surf. Sci.*, 253(5) (2006) 2618.
2. G. Qiao, T. Jing, N. Wang, Y.W. Gao, X. Zhao, J.F. Zhou, and W. Wang, *Electrochim. Acta*, 51 (1) (2005) 85.
3. J. Vazquez-Arenas, T. Treeratanaphitak, and M. Pritzker, *Electrochim. Acta.*, 62 (2012) 63.
4. D.H. Kim, *J. Electrochem. Soc.*, 142(11) (1995) 3763.
5. L.P. Wang, Y. Gao, Q.J. Xue, H.W. Liu, and T. Xu, *Appl. Surf. Sci.*, 242 (3-4) (2005) 326.
6. B. Li and W. Zhang, *Int. J. Electrochem. Sci.*, 12(8) (2017) 7017.
7. L. Shi, C.F. Sun, P. Gao, F. Zhou, and W.M. Liu, *Appl. Surf. Sci.*, 252 (10) (2006) 3591.
8. M. Srivastava, V.K.W. Grips, and K.S. Rajam, *Appl. Surf. Sci.*, 253 (8) (2007) 3814.
9. S.M.L. Baghal, A. Amadeh, and M.H. Sohi, *Mat. Sci. Eng. A-struct.*, 542 (2012) 104.
10. A. Hefnawy, N. Elkhoshkhany, and A. Essam, *J. Alloy. Compd.*, 735 (2018) 600.
11. W. Jiang, L.D. Shen, M.Y. Xu, Z.W. Wang, and Z.J. Tian, *J. Alloy. Compd.*, 791 (2019) 847.
12. K. Arunsunai Kumar, G. Paruthimal Kalaignan, and V. S. Muralidharan, *Ceram. Int.*, 39 (3) (2013) 2827.
13. C.Y. Ma, D.Q. Zhao, F.F. Xia, H. Xia, T. Williams, and H.Y. Xing, *Ceram. Int.*, 46(3) (2020) 1500.
14. F. Xia, Q. Li, C. Ma, and X. Guo, *Ceram. Int.*, 46 (2) (2020) 2500.
15. C. Sun, X. Liu, C. Zhou, C. Wang, and H. Cao, *Ceram. Int.*, 45 (1) (2019) 1348.
16. Y. Yang, and Y.F. Cheng, *Electrochim. Acta.*, 109 (2013) 638.
17. F. Xia, X. Zhao, M. Jiang, and C. Ma, *AIP Adv.*, 9 (2019) 065310.
18. F.F. Xia, M. Huang, C.Y. Ma, and H.Y. Yin, *J. Funct. Mater.*, 44 (16) (2013) 2429.
19. H.N. Vatan, R.E. Kahrizsangi, and M.K. Asgarani, *Prot. Met. Phys. Chem.*, 52 (5) (2016) 859.
20. D. Ning, A. Zhang, M. Murtaz, and H. Wu, *J. Alloy. Compd.*, 777 (2019) 1245.
21. B. Li, W. Zhang, W. Zhang, and Y. Huan, *J. Alloy. Compd.*, 702 (2017) 38.
22. N. Shakibi Nia, J. Creus, X. Feaugas, and C. Savall, *Appl. Surf. Sci.*, 370 (2016) 149.
23. M. Sajjadnejad, H. Omidvar, M. Javanbakht, and A. Mozafari, *J. Alloy. Compd.*, 704 (2017) 809.
24. F.F. Xia, C. Liu, F. Wang, M.H. Wu, J.D. Wang, H.L. Fu, and J.X. Wang, *J. Alloy. Compd.*, 490 (2010) 431.
25. B. Li and W. Zhang, *Ceram. Int.*, 44 (2018) 19907.
26. B. Babak. *Surf. Coat. Technol.*, 275 (2015) 324.
27. F.F. Xia, W.C. Jia, C.Y. Ma, R. Yang, Y. Wang, and M. Potts, *Appl. Surf. Sci.*, 434 (2018) 228.
28. F. Xia, J. Tian, W. Wang, and Y. He, *Ceram. Int.*, 42 (2016) 13268.
29. C. Ma, M. Jiang, and F. Xia, *Surf. Rev. Lett.*, 24 (5) (2017) 1750063.
30. N.P. Wasekar, L. Bathini, and G. Sundararajan, *J. Mater. Eng. Perform.*, 27 (2018) 5236.
31. H. Gül, F. Kılıç, S. Aslan, A. Alp, and H. Akbulut, *Wear*, 267 (2009) 976.
32. Y.N. Bekish, S.K. Poznyak, L.S. Tsybulskaya, and T.V. Gaevskaya, *Electrochim. Acta*, 55 (2010) 2223.